

Reassessing evidence of life in 3,700-million-year-old rocks of Greenland

Abigail C. Allwood^{1*}, Minik T. Rosing², David T. Flannery¹, Joel A. Hurowitz^{3*} & Christopher M. Heirwegh¹

The Palaeoarchean supracrustal belts in Greenland contain Earth's oldest rocks and are a prime target in the search for the earliest evidence of life on Earth. However, metamorphism has largely obliterated original rock textures and compositions, posing a challenge to the preservation of biological signatures. A recent study of 3,700-million-year-old rocks of the Isua supracrustal belt in Greenland described a rare zone in which low deformation and a closed metamorphic system allowed preservation of primary sedimentary features, including putative conical and domical stromatolites¹ (laminated accretionary structures formed by microbially mediated sedimentation). The morphology, layering, mineralogy, chemistry and geological context of the structures were attributed to the formation of microbial mats in a shallow marine environment by 3,700 million years ago, at the start of Earth's rock record. Here we report new research that shows a non-biological, post-depositional origin for the structures. Three-dimensional analysis of the morphology and orientation of the structures within the context of host rock fabrics, combined with texture-specific analyses of major and trace element chemistry, show that the 'stromatolites' are more plausibly interpreted as part of an assemblage of deformation structures formed in carbonate-altered metasediments long after burial. The investigation of the structures of the Isua supracrustal belt serves as a cautionary tale in the search for signs of past life on Mars, highlighting the importance of three-dimensional, integrated analysis of morphology, rock fabrics and geochemistry at appropriate scales.

Earth's earliest fossil assemblages are important for understanding the origins of life on Earth and, by analogy, how and where to search for signs of primitive life in the rock record of other planets². The oldest widely accepted evidence of life on Earth is in marine metasedimentary rocks of the Pilbara Craton, Australia, in the form of a microbial stromatolite reef^{3,4} and fossil biofilms⁵ of the 3,450-million-year-old (Myr) Strelley Pool Formation. Putative microfossils⁶ (Strelley Pool Formation) and stromatolites (3,490-Myr-old Dresser Formation)⁷ also occur in the Pilbara Craton, but their biogenicity is equivocal⁸. In Greenland, geochemical features compatible with microbial activity exist^{9,10}, but their interpretation has been questioned^{11–13}. The presence of 3,700-Myr-old stromatolites in Greenland's Isua supracrustal belt (ISB), if true, would represent an entirely new and compelling type of biosignature in Earth's oldest rocks and establish the start of the fossil record 200 Myr earlier than previously thought¹.

The putative stromatolites, discovered approximately 150 km northeast of Nuuk (Extended Data Fig. 1), were described¹ as elongate cones and domes 1–4 cm high, with apices pointing upward relative to overturned sedimentary bedding. Combining those attributes with: (1) internal stromatolitic lamination that is continuous across the crests of the structures; (2) diverse morphologies similar to younger stromatolites; (3) associated shallow-water sedimentary features, including sedimentary onlap; (4) differences in chemical composition inside the structures compared to surrounding sedimentary rock; (5) the presence of low temperature dolomite; and (6) seawater-like rare earth element

and yttrium (REE + Y) composition of the dolomite, it was proposed in the previous study¹ that the structures are stromatolites produced by microbial communities in a shallow marine, carbonate-platform environment similar to the stromatolites in the Strelley Pool Formation^{3,4}. Preservation of these features was attributed to an approximately 30-m × 70-m low-deformation lacuna in the hinge of an anticline¹.

We located the discovery outcrops using data from the previous study¹. Site A consists of brownish-grey layered dolomitic rock, with light-grey triangular features mostly oriented apex-up relative to the overturned layering. However, some are apex-down (Fig. 1a and Extended Data Fig. 2c), which is inconsistent with upward growth of the structures from a palaeo-seafloor. Dolomitic breccia nearby (site C) was previously interpreted as a tempestite (storm deposit), which in turn was taken as evidence of a shallow-water, ice-free sedimentary environment¹. However, a wider view of the outcrop shows ductile and brittle deformation of the clasts, including extreme elongation when viewed from the side (Extended Data Fig. 3), indicating that the breccia has a tectonic origin and has no bearing on water depth, ice or other sedimentary conditions.

A sample was acquired approximately 0.5 m from the original 'stromatolite' sample site of site A¹⁴, including one of the triangular structures (Extended Data Fig. 2). Cut parallel to the weathered face (face 1, Fig. 1c–e), the sample shows irregularly layered light- and medium-grey quartz-dolomite layers with dark micaceous layers and foliation. An array of millimetre- to centimetre-scale convex-up features, of which the triangle structure is the largest, all have subparallel axial planes (Fig. 1c, d). Notably, the base of the triangular structure is also convex-up and conformable with small convex-up features in the underlying quartzose layers. The fabric is extensively disrupted by planar discontinuities, or spaced cleavage, subparallel to the axial planes of the convex-up features (Fig. 1c). By contrast, when viewed orthogonally (face 2, Fig. 1b), the rock shows flat, even layering without any stromatolites, bumps or irregularities (Fig. 1b, e and Extended Data Fig. 4).

Such orientation-dependent, contrasting fabrics are inconsistent with sedimentary processes. Rather, they are typical deformation fabrics found in a multi-layered rock that has been shortened in one direction (parallel to layering), producing minor folds, cleavage and other compressional features similar to those observed on face 1; and substantially lengthened in an orthogonal direction, producing extensional rod-like features such as those observed on face 2. The type of deformation indicated is consistent with the structural setting of the rock, within the hinge of an anticline¹.

Accordingly, cuts parallel to face 1 show that the 'stromatolites' are not cones or elongate cones, but ridges extending at least 10 cm (our sampling depth) into the rock, aligned with the lengthening direction. The ridges probably extend further, given the extreme elongation of the rock fabric observed in the outcrop. Photographs published in the previous study¹ suggest that the structure that they sampled is also ridge-shaped. Although ridge morphology alone does not preclude biological origins, it is easier to produce ridges abiotically than cones^{3,4}. More importantly, a deformational origin is more plausible given the

¹Jet Propulsion Laboratory, California Institute of Technology, Pasadena, CA, USA. ²Natural History Museum of Denmark, University of Copenhagen, Copenhagen, Denmark. ³Department of Geosciences, Stony Brook University, Stony Brook, NY, USA. *e-mail: abigail.c.allwood@jpl.nasa.gov; joel.hurowitz@stonybrook.edu

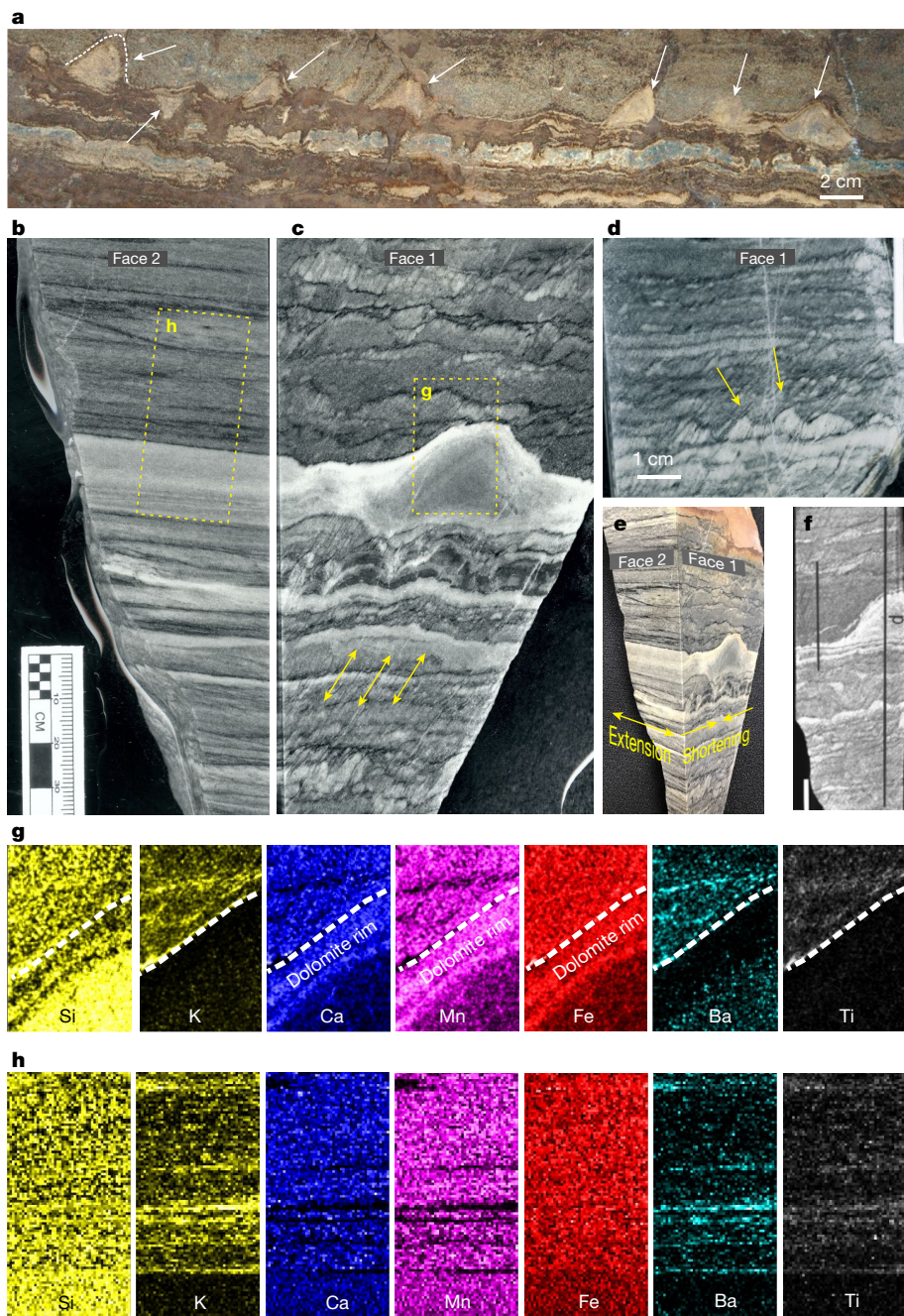


Fig. 1 | Putative stromatolites of Greenland. **a**, Seven structures in outcrop (arrows, white dashed line). **b–d**, Sample from site A. **b**, Face 2 shows even, parallel layering. **c, d**, Face 1 shows irregularly layered fabric with planar discontinuities (arrows in **c**) and convex-up features (two yellow arrows in **d**). Yellow dashed boxes indicate panels expanded in **g**, **h** as indicated. **e**, Oblique view of the sample. **f**, Sample from the previous study¹, equivalent to face 1. Lines indicate the path of X-ray fluorescence

scans in the previous study¹. The 'd' denotes their scan through the stromatolite. **g**, PIXL element maps of stromatolite and matrix (yellow box in **c**). Dashed line marks the edge of the structure, below which the composition shows a gradient from a Ca–Mn–Fe-rich rim to a Si-rich interior. **h**, PIXL maps of the light-grey layer (yellow box in **b**) show elemental composition, including Ti and K depletion, identical to the 'stromatolite'.

alignment of the ridges with the lengthening direction indicated by the rock fabrics.

The previous study¹ included outcrop photographs of thin, recessive laminae that tangentially truncate against a structure, which the authors use as evidence of seafloor growth of a stromatolite. However, similar truncation occurs in our sample where micaceous foliation terminates against the triangular structure—an observation that is consistent with the presence of a rigid object (the quartzose ridge) in a ductilely deforming rock, leading to deflection and pressure solution of the mica and carbonate foliation on the shortening side. Tangentially truncated laminae observed in the thin section¹ occurred at site B. However, the

putative stromatolitic structures from site B illustrated in the previous study¹ are very different from those at site A: the published image only shows an undulose lithologic contact (Fig. 2b of the previous study¹).

PIXL (planetary instrument for X-ray lithochemistry) micro-X-ray fluorescence maps of elemental composition cast new light on putative evidence for biological activity¹. First, maps of the distribution of the elements calcium, iron and manganese show that 'stromatolitic' lamination internal to the structures is actually a dolomitic alteration rim on a quartzose interior (Fig. 1g) and that there is no other compositional relict of internal lamination in the structures. Second, titanium and potassium are depleted not only in the 'stromatolites' but also throughout the

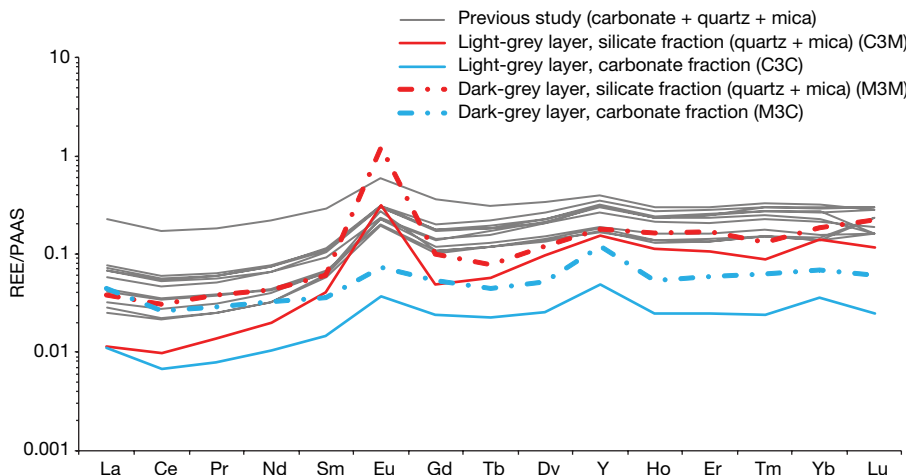


Fig. 2 | Relative abundance of REE + Y for different components of the Isua rock samples. Blue and red lines, our sample, which was separated into silicate and carbonate fractions. Grey lines, sample analysed in the previous study¹, combining carbonate and silicate. All have light rare earth elements (LREE) element depletion ($\text{Pr}/\text{Yb} \ll 1$), Y/Ho ratio of ≥ 30 ,

quartzose layers (Fig. 1h), owing to the fact that they have considerably less potassium- and titanium-bearing mica compared to the dark layers. Finally, the iron and silicon maps show iron-rich/silicon-poor dark layers and silicon-rich/iron-poor light layers, suggesting that the rock may have originally consisted of intercalated cherty and iron-rich strata, which is consistent with previous studies and our observations of carbonate-altered banded iron formation and cherty metasediments in nearby outcrops¹⁵.

In the previous study, low-temperature dolomite formation was inferred from C and O isotopes, and this was interpreted as evidence of biogenic dolomite formation in the sedimentary environment¹. However, the role of microbes in low-temperature dolomite formation is equivocal¹⁶. Furthermore, low temperature does not preclude secondary origins—an hypothesis supported by the presence of dolomite alteration rims observed in PIXL maps (Fig. 1g).

The REE + Y geochemistry of dolomite was mentioned as evidence of primary marine carbonate sedimentation in the previous study¹. However, synchrotron X-ray fluorescence element maps show that the 800-μm-wide laser-ablation inductively coupled plasma-mass spectroscopy scans collected by Nutman et al.¹ would have sampled a mixture of dolomite, quartz and micas. Therefore, their REE + Y patterns cannot be attributed to dolomite alone. Micas, in particular, are important trace element carriers in these rocks (Extended Data Fig. 6 and Supplementary Information).

To resolve this uncertainty, we separated carbonate and silicate (quartz and mica) fractions (Extended Data Fig. 5) by acid digestion and measured the REE + Y by mass spectroscopy (Fig. 2 and Extended Data Table 1). Both have REE + Y patterns broadly consistent with the properties of Archean to Paleoproterozoic seawater^{17–19}. However, the overall abundance is higher in the silicates than carbonates, and higher in the mica-rich silicate sample than in the mica-poor silicate sample. These observations can be attributed to a high REE + Y concentration in micas. The silicate REE + Y pattern also has a larger positive Eu anomaly than the carbonate, indicating a different origin of the silicates compared to carbonate. Given the observed carbonate alteration of quartz (Fig. 1g), the most plausible interpretation is that the carbonate REE + Y composition was inherited from diagenetic and/or metasomatic fluids. In summary, the texture-specific distribution of major and minor elements, and the REE + Y composition of the rocks are consistent with original deposition in a marine environment, followed by secondary carbonate alteration any time between early diagenesis²⁰ and late carbonate metasomatism—the latter process having been well-documented in nearby ISB meta-sedimentary rocks¹⁵.

positive La and Eu anomalies, broadly consistent with Archean seawater origins. However, carbonate and silicate fractions are different in abundance (due to mica) and pattern, including a more pronounced positive Eu anomaly in the silicate fractions. PAAS, post-Archean Australian Shale composite.

Therefore, we propose that none of the previously published results support the interpretation of the ISB structures as stromatolites: they lack internal lamination and we found no evidence of synsedimentary growth. Their triangular ridge shape is not an indicator of biogenicity and they do not exhibit unique chemical compositions that indicate a localized microbial influence on the sedimentary processes¹. We agree that the host rock protolith formed in a marine environment; however, there is no evidence for shallow water depth, and there is no unambiguous evidence that carbonate was part of the primary sedimentary assemblage. The inherent attributes of the structures, their geological setting in a fold hinge, the deformation fabrics observed in the host rock, and the shape and alignment of the structures within the overall rock fabrics—all indicate non-biological origins. In our view, it is very reasonable to interpret the ISB structures as products of structural deformation and carbonate alteration of layered rocks. On the other hand, we believe that the current evidence does not support the interpretation of these structures as 3,700-Myr-old stromatolites.

Online content

Any methods, additional references, Nature Research reporting summaries, source data, statements of data availability and associated accession codes are available at <https://doi.org/10.1038/s41586-018-0610-4>.

Received: 21 December 2017; Accepted: 31 August 2018;

Published online 17 October 2018.

- Nutman, A. P., Bennett, V. C., Friend, C. R. L., Van Kranendonk, M. J. & Chivas, A. R. Rapid emergence of life shown by discovery of 3,700-million-year-old microbial structures. *Nature* **537**, 535–538 (2016).
- Allwood, A. et al. Conference summary: life detection in extraterrestrial samples. *Astrobiology* **13**, 203–216 (2013).
- Allwood, A. C., Walter, M. R., Kamber, B. S., Marshall, C. P. & Burch, I. W. Stromatolite reef from the Early Archean era of Australia. *Nature* **441**, 714–718 (2006).
- Allwood, A. C., Walter, M. R., Burch, I. W. & Kamber, B. S. 3.43 billion-year-old stromatolite reef from the Pilbara Craton of Western Australia: ecosystem-scale insights to early life on Earth. *Precambr. Res.* **158**, 198–227 (2007).
- Allwood, A. C. et al. Controls on development and diversity of Early Archean stromatolites. *Proc. Natl. Acad. Sci. USA* **106**, 9548–9553 (2009).
- Sugitani, K. et al. Biogenicity of morphologically diverse carbonaceous microstructures from the ca. 3400 Ma Strelley pool formation, in the Pilbara Craton, Western Australia. *Astrobiology* **10**, 899–920 (2010).
- Walter, M. R., Buick, R. & Dunlop, S. R. Stromatolites 3,400–3,500 Myr old from the North Pole area, Western Australia. *Nature* **284**, 443–445 (1980).
- Mojzsis, S. J. et al. Evidence for life on Earth before 3,800 million years ago. *Nature* **384**, 55–59 (1996).
- Rosing, M. T. ^{13}C -depleted carbon microparticles in >3700-Ma sea-floor sedimentary rocks from West Greenland. *Science* **283**, 674–676 (1999).

10. Schidlowski, M., Appel, P. W., Eichmann, R. & Junge, C. E. Carbon isotope geochemistry of the 3.7×10^9 -yr-old Isua sediments, West Greenland: implications for the Archaean carbon and oxygen cycles. *Geochim. Cosmochim. Acta* **43**, 189–199 (1979).
11. van Zuilen, M. A., Lepland, A. & Arrhenius, G. Reassessing the evidence for the earliest traces of life. *Nature* **418**, 627–630 (2002).
12. Lindsay, J. F. et al. The problem of deep carbon—an Archean paradox. *Precambr. Res.* **143**, 1–22 (2005).
13. Shields, G. & Veizer, J. Precambrian marine carbonate isotope database: version 1.1. *Geochem. Geophys. Geosyst.* **3**, 1–12 (2002).
14. Nutman, A., Van Kranendonk, M. *Sampling of the World's Oldest Stromatolites from Isua (Greenland): Damage to a Globally-Unique Locality*. Technical Report (2017).
15. Fedo, C. M., Myers, J. S. & Appel, P. W. U. Depositional setting and paleogeographic implications of Earth's oldest supracrustal rocks, the >3.7 Ga Isua Greenstone belt, West Greenland. *Sediment. Geol.* **141–142**, 61–77 (2001).
16. Machel, H. G. Concepts and models of dolomitization: a critical reappraisal. *Geol. Soc. Spec. Publ.* **235**, 7–63 (2004).
17. Bau, M. & Dulski, P. Distribution of yttrium and rare-earth elements in the Penge and Kuruman iron-formations, Transvaal Supergroup, South Africa. *Precambr. Res.* **79**, 37–55 (1996).
18. Nutman, A. P., Friend, C. R. L., Bennett, V. C., Wright, D. & Norman, M. D. >3700 Ma pre-metamorphic dolomite formed by microbial mediation in the Isua supracrustal belt (W. Greenland): simple evidence for early life? *Precambr. Res.* **183**, 725–737 (2010).
19. Planavsky, N. et al. Rare earth element and yttrium compositions of Archean and Paleoproterozoic Fe formations revisited: new perspectives on the significance and mechanisms of deposition. *Geochim. Cosmochim. Acta* **74**, 6387–6405 (2010).
20. Qing, H. & Mountjoy, E. W. Rare earth element geochemistry of dolomites in the Middle Devonian Presqu'ile barrier, Western Canada Sedimentary Basin: implications for fluid–rock ratios during dolomitization. *Sedimentology* **41**, 787–804 (1994).

Acknowledgements Part of this research was carried out at the Jet Propulsion Laboratory, California Institute of Technology, under a contract with the National Aeronautics and Space Administration (NASA). Funding for the work was provided by the NASA Mars 2020 PIXL flight project. We thank the Government of Greenland, Ministry of Mineral Resources for provision of

access to the field sites, sampling permits and specifically geologist A. Juul-Nielsen for accompanying us on the field expedition, participating in discussions to determine an acceptable sampling strategy, and approving the final sample collection; T. Elam for providing the PIQUANT quantification code and descriptions of its architecture for the PIXL prototype; J. Thieme and E. Fogelqvist for assistance with data collection and reduction at the SRX beamline; T. Rasbury and K. Wootton for assistance with sample digestion and REE + Y analysis; I. Burch for field assistance including sample acquisition; K. Bourke for cutting and polishing the rock samples; and I. Fast for assistance in the field. J.A.H. acknowledges partial support from the Stony Brook University-Brookhaven National Laboratory Seed Grant program.

Reviewer information *Nature* thanks M. M. Tice, M. van Zuilen and the other anonymous reviewer(s) for their contribution to the peer review of this work.

Author contributions A.C.A. led the research and field expedition, determined analytical strategy for samples, interpreted data, analysed the structures and wrote the manuscript. M.T.R. coordinated field logistics, including sampling permits and inclusion of Greenland government staff in the fieldwork and sampling operations, made field observations, interpreted metamorphic history, provided regional geologic context and contributed to manuscript writing. J.A.H. performed synchrotron X-ray fluorescence analyses, REE + Y analyses and interpreted geochemical data, contributed to manuscript writing and helped to write the Methods. D.T.F. acquired and analysed PIXL maps, performed thin section petrography and contributed to manuscript revisions. C.M.H. processed the PIXL data used in elemental maps and helped to write the Methods.

Competing interests The authors declare no competing interests.

Additional information

Extended data is available for this paper at <https://doi.org/10.1038/s41586-018-0610-4>.

Supplementary information is available for this paper at <https://doi.org/10.1038/s41586-018-0610-4>.

Reprints and permissions information is available at <http://www.nature.com/reprints>.

Correspondence and requests for materials should be addressed to A.C.A. or J.A.H.

Publisher's note: Springer Nature remains neutral with regard to jurisdictional claims in published maps and institutional affiliations.

METHODS

Data reporting. No statistical methods were used to predetermine sample size. The experiments were not randomized and the investigators were not blinded to allocation during experiments and outcome assessment.

PIXL analysis at the Jet Propulsion Laboratory. PIXL (planetary instrument for X-ray lithochemistry) is a microfocus X-ray fluorescence instrument developed at the Jet Propulsion Laboratory to fly aboard NASA's Mars 2020 rover mission. The PIXL engineering prototype used in this study employs a MoXtek 12-Watt 60-kV MAGPRO RH X-ray tube, in 180° emission geometry, mated with an XOS (6319) glass polycapillary focusing optic. The optic delivers a sub-millimetre (around 100 µm diameter at 7 keV) focused X-ray beam spot at a nominal 2-cm stand-off distance from the target. Two Ketek Vetus H50 AXAS-D detectors (model: D5C2T0-H50-ML9BEV), oriented at 20° relative to the beam axis, provide a near-backscatter geometry for optimized X-ray detection. Analogue-to-digital conversion of X-ray signals and multi-channel binning of pulses is performed by the Ketek-built electronics. Data were acquired using an in-house-designed acquisition software built using a National Instruments LabVIEW platform.

Measurements of the Greenland rock were performed in air using 28 kV/100 µA X-ray tube-operating conditions. The rock sample was cut, polished and cleaned. The data of Fig. 1g were acquired by rastering the X-ray beam across the sample surface in *x* and *y* directions in 100-µm steps, with 15-s integration at each step, to produce a 10 × 15-mm² image containing 15,000 data points. For Fig. 1h, a 200-µm step size was selected and a 10 × 20-mm² area, containing 5,000 data points, was imaged.

To accurately identify the elements present, all of the spectra in each map were summed together to produce a whole-map summed spectrum. Principal elemental peaks of the major elements of interest were identified and peak areas under the characteristic X-ray peaks were derived using the in-house software package PIQUANT²¹, designed to process and fit spectral data generated by PIXL. PIQUANT uses a rigorously applied linear least-squares spectrum peak-fitting approach to ensure robust identification of elements, the fitting routine of PIQUANT applies Gaussian functions to each of the X-ray lines that describe a peak. The analytic integral of the combined Gaussians produces the net peak intensity. Peak intensity is one of the fitted variables. Also variable are two parameters associated with the peak widths and two more to describe the channel bin-to-peak energy conversion. The 'noise' corresponding primarily to the bremsstrahlung background that underlies the X-ray peaks is fitted separately using a SNIP¹⁷-fitting algorithm. The background contribution is subtracted as part of deriving the net peak intensities. This approach enables accurate distinction of element peaks even when the peaks overlap. In the Greenland rock maps, the Ba L α X-ray peak (4.47 keV) and Ti K α X-ray peak (4.51 keV) are an example of this. Both appear almost as part of one peak, broadened by the contribution and with 40-eV separation of the two elemental lines. With PIQUANT, the individual lines are distinguished, given that the line energies are constrained to a fixed energy and the peak widths and channel energy calibration parameters are constrained by values derived from the dominant lines of neighbouring elements (for example, Ca and Fe). Harnessing these constraints enables separation of Ti from Ba.

One challenge that persists through these spectra is that coherent scatter diffraction peaks appear in the energy range of spectra in which Ti and Ba peaks reside. Their presence has the potential to be registered falsely as a characteristic X-ray response. The PIQUANT software does not yet possess a treatment process that would allow for correction of this contribution. Therefore, a very small amount of data from this region may represent diffraction scatter instead of a X-ray response.

PIQUANT utilizes the databases from a previous study²², although a number of those databases have been, or are currently being, modified.

REE + Y analyses at Stony Brook University. Four samples were prepared and analysed by inductively coupled plasma mass spectrometry (ICP-MS) for their rare earth element (REE) and Y concentrations (REE + Y). A slab of the sample shown in Fig. 1b, c was sectioned with a tile saw (Extended Data Fig. 5) to separate a portion of the carbonate-rich rim on the light-grey part of the rock (subsample 'C') and a portion of the overlying dark-grey part of the rock (subsample 'M'). These two subsamples were hand crushed in a ceramic mortar and then powdered in an agate shatterbox. Half a gram of each powder was weighted out and sonicated with 2% nitric acid for 30 min to leach carbonate from the samples. The supernatant was then removed, diluted and analysed by ICP-MS; these are samples C3C and M3C. About 40 mg (dry weight) of the remaining leached sediment was then dried and dissolved in a mixture of hydrofluoric and nitric acid for 12 h in sealed Teflon vials on a hotplate at around 120 °C. They were then dried and dissolved in aqua regia for 12 h in sealed Teflon vials on a hotplate at around 120 °C.

Once completely dissolved, the aqua regia was dried off and the samples were reconstituted in nitric acid, which was then diluted and analysed by ICP-MS; these are samples C3M and M3M.

Elemental concentration analyses were performed in the FIRST (Facility for Isotope Research and Student Training) Laboratory in the Department of Geosciences at Stony Brook University on an Agilent 7500cx quadrupole ICP-MS. Samples were diluted to match to the signal of mixed calibration standards and unknown concentrations were calculated based on standard calibration curves, with standards run frequently between unknowns to monitor for drift in signal intensity. The U.S.G.S. Cody shale standard, SCO-1, was used to calculate the elemental concentrations for these samples. The REEs and Y concentrations in parts per million (p.p.m.) are shown in Extended Data Table 1. Concentrations were calculated for the carbonate leach of each sample assuming only carbonate was dissolved in 2% nitric acid using Ca and Mg concentrations to calculate the carbonate mass dissolved.

High-resolution X-ray fluorescence mapping at NSLS-II. High-resolution synchrotron X-ray fluorescence (XRF) spectra were collected on the Sub-micron Resolution X-ray spectroscopy (SRX) beamline at the National Synchrotron Light Source 2 (NSLS-II) at the Brookhaven National Laboratory. The capabilities of the SRX beamline have previously been described^{23,24}. In brief, SRX is a hard X-ray microprobe that performs scanning micro-fluorescence microscopy (μ -XRF) and X-ray absorption near-edge structure (μ -XANES) analysis using the high-brightness NSLS-II as a source of incident radiation. The SRX optics allow investigation of elemental distribution and chemical speciation at the sub-micrometre scale. For our analyses, we used an incident beam energy of 12 keV. The beam was focused to a spot size of 1 µm and XRF spectra were collected for 0.6 s at each spot. Motorized stages were used to move the sample under the beam with a 2-µm step size, thus generating a two-dimensional map of the elemental composition of this sample. Fluorescent X-rays were detected using an energy dispersive X-ray detector (Hitachi Vortex silicon drift detector). We analysed two areas, called 'map 1' and 'map 2' (Extended Data Fig. 6, Supplementary Information), on a cut and polished slab sample from locality A. This slab contains one of the putative stromatolite-like features, bounded above and below by alternating light and dark layers. XRF spectra for map 1 were collected on a 1–2 mm thick dark-black layer bounded above and below by thicker grey coloured layers. XRF spectra for map 2 were collected from within the core of the stromatolite-like feature. The dimensions of the maps are 200 × 200 µm² and 125 × 125 µm², respectively. To generate element maps, the individual X-ray spectra from each map were first summed into single bulk spectra (that is, one for map 1 and another for map 2) and fitted using the PyXRF analysis package developed at NSLS-II²⁵. PyXRF uses a nonlinear least-squares method to determine global parameters such as peak width, energy calibration values, parameters related to the Compton and elastic scattering peaks, and element identities. Once elements were identified in the summed spectra, individual spectra were searched for those elements, their peak areas were fitted, and maps of elemental distribution and fluorescence intensity were generated.

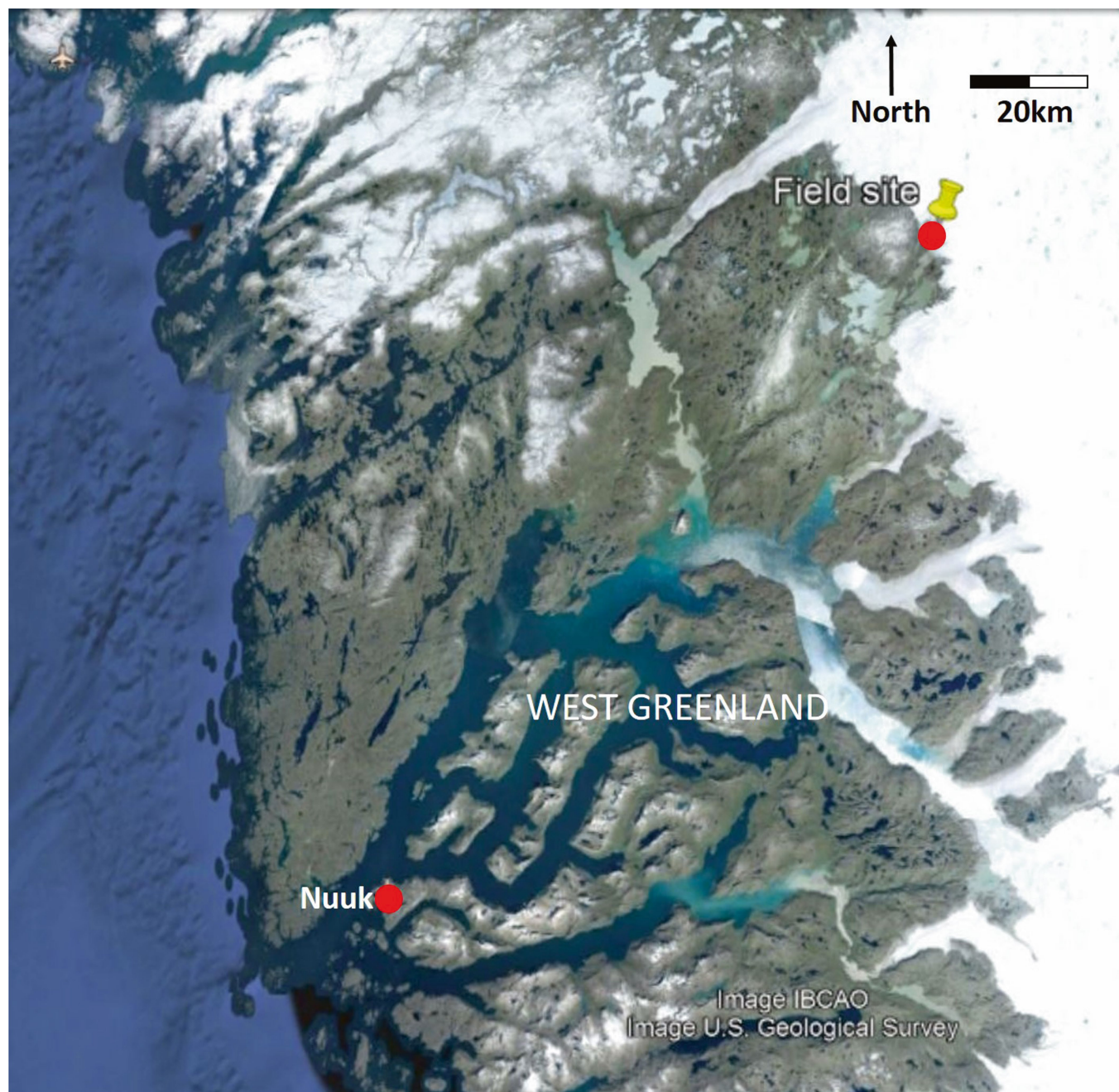
Reporting summary. Further information on research design is available in the Nature Research Reporting Summary linked to this paper.

Code availability. PIQUANT software used in the study is available from the corresponding authors upon reasonable request.

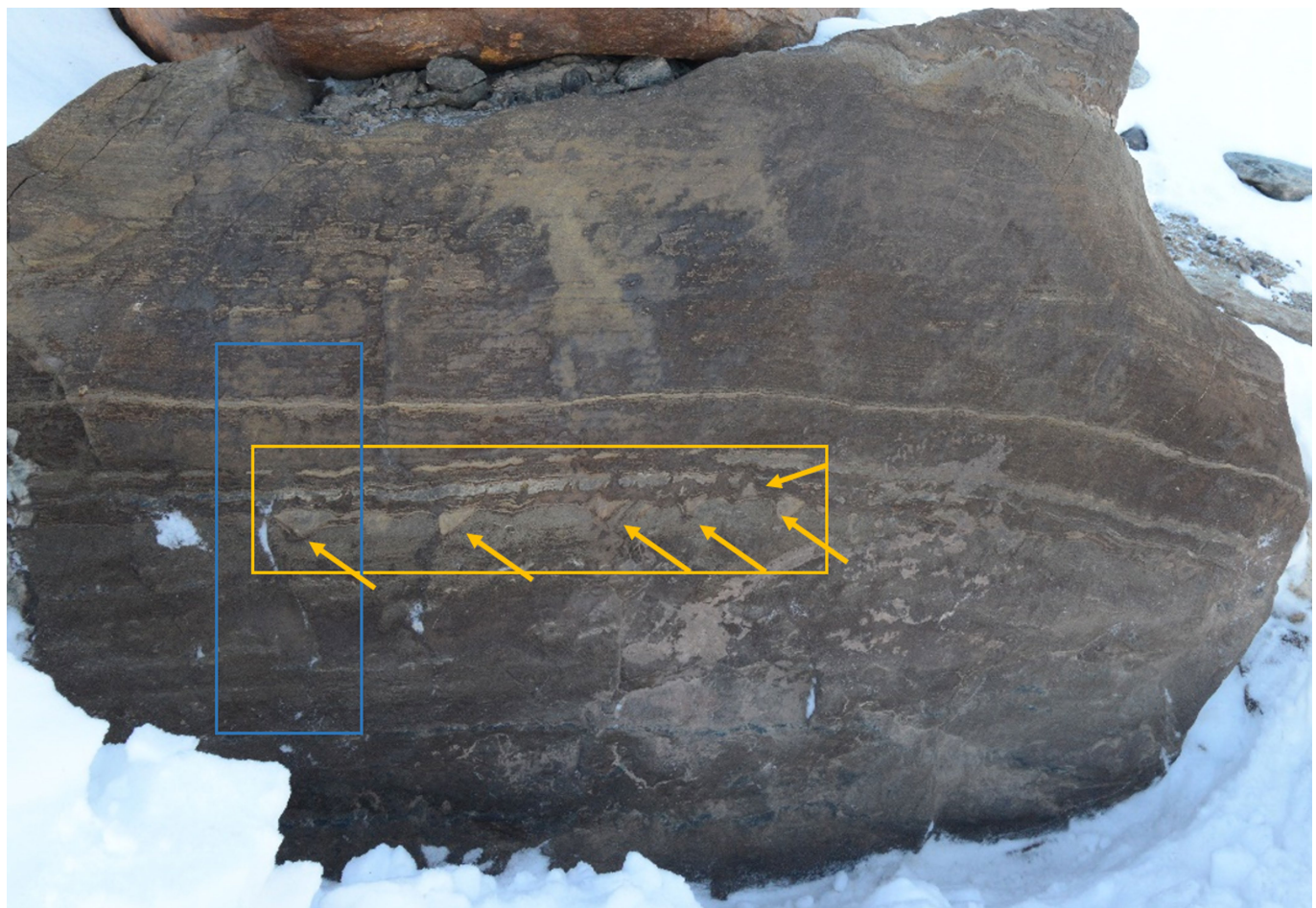
Data availability

The datasets generated during and/or analysed during the current study are available from the corresponding authors upon reasonable request.

21. Heirwegh, C. M., Elam, W. T., Flannery, D. T. & Allwood, A. C. An empirical derivation of the X-ray optic transmission profile used in calibrating the Planetary Instrument for X-ray Lithochemistry (PIXL) for Mars 2020. *Powder Diffr.* 162–165 (2018).
22. Elam, W. T. et al. A new atomic database for the X-ray spectroscopic calculations. *Radiat. Phys. Chem.* **63**, 121–128 (2002).
23. De Andrade, V. et al. The sub-micron resolution X-ray spectroscopy beamline at NSLS-II. *Nucl. Instrum. Methods Phys. Res. A* **649**, 46–48 (2011).
24. Chen-Wiegert, Y. C. K. et al. Early science commissioning results of the sub-micron resolution X-ray spectroscopy beamline (SRX) in the field of materials science and engineering. In *Proc. 23rd International Conference on X-Ray Optics and Microanalysis* (eds Thieme, J. & Siddons, D. P.) (ICXOM23, American Institute of Physics, 2016).
25. Li, L., Yan, H., Xu, W., Yu, D. & Heroux, A. *PyXRF: Python-based X-ray fluorescence analysis package*. *Proc. 10389 X-Ray Nanoimaging, Instruments and Methods III* 103890U (SPIE Optical Engineering & Applications, 2017).

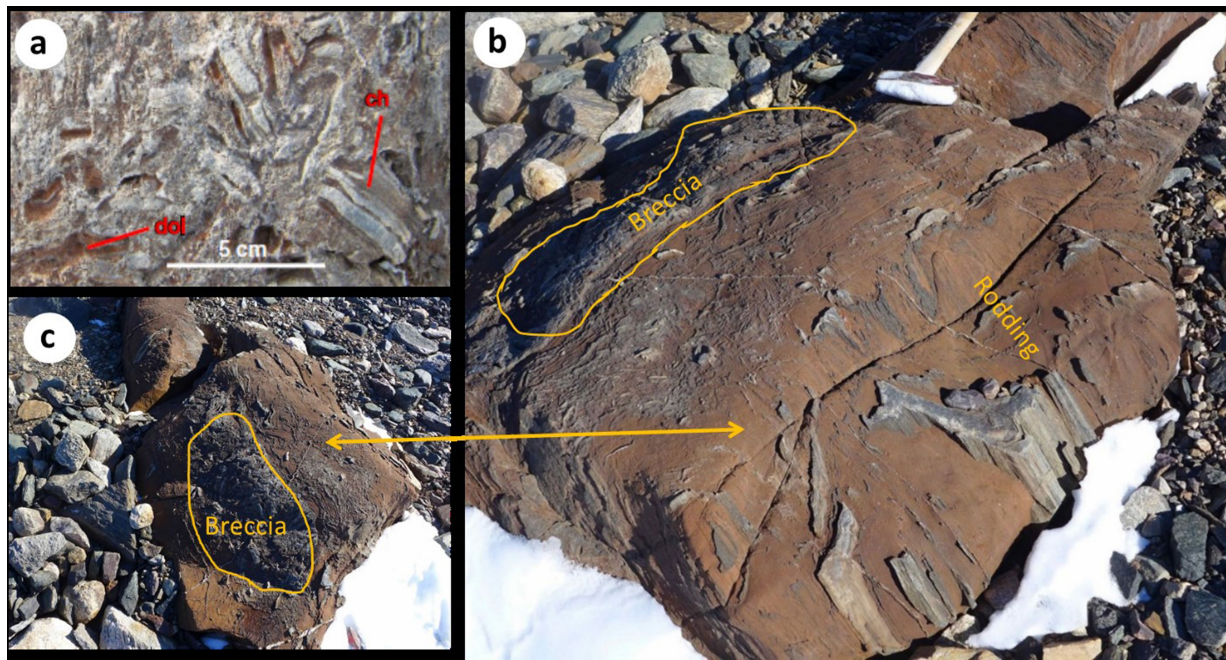


Extended Data Fig. 1 | Satellite image showing the approximate outline and location of the Isua Structural Belt and the study area. The satellite image of the study area. The image was obtained from Google Maps.



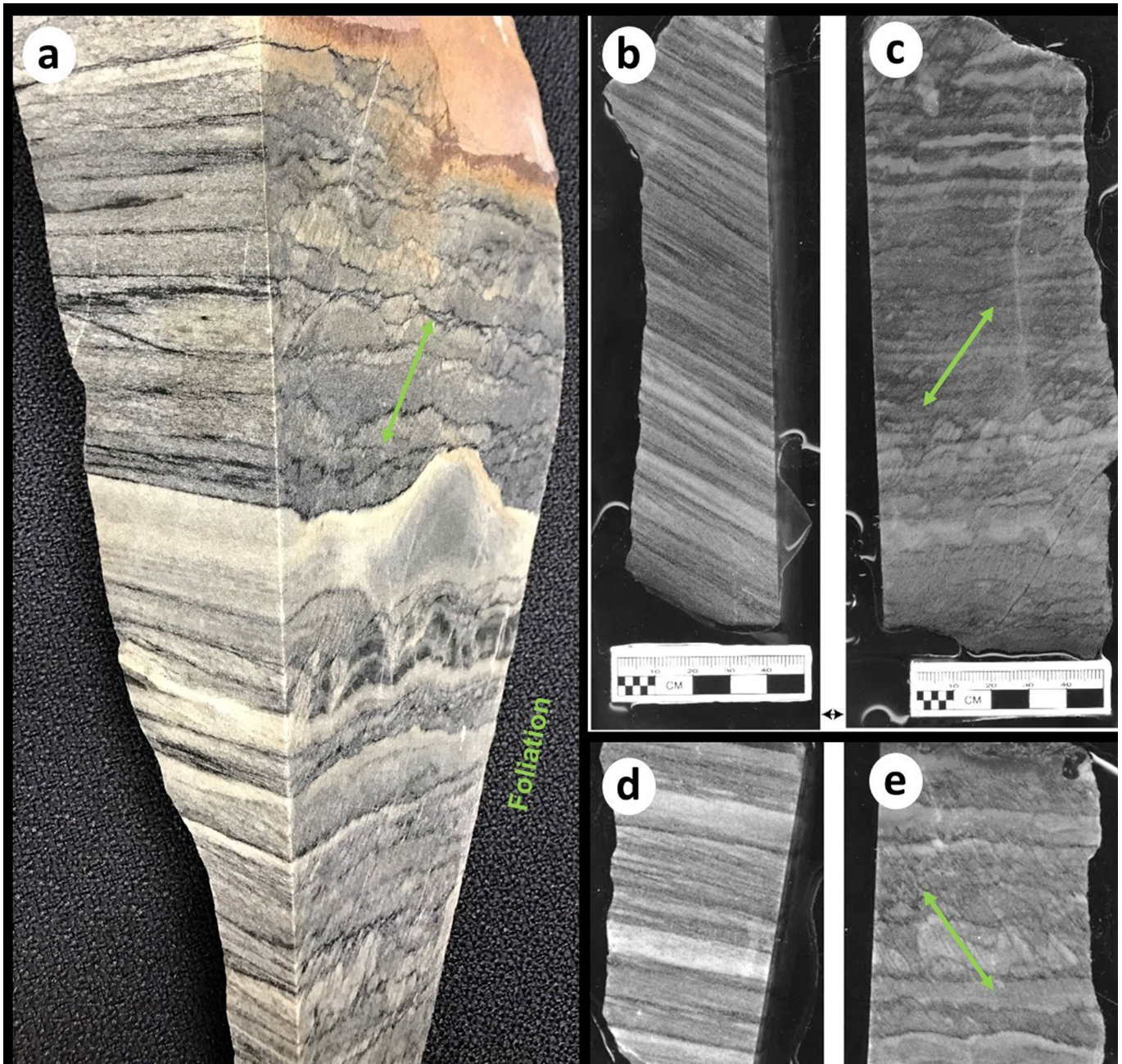
Extended Data Fig. 2 | Putative stromatolites of the ISB at site A. Yellow arrows point to triangular shapes with apices mostly pointing down relative to layering. Note, the stratigraphy was inverted, as the layers have

been overturned¹. Each of the triangles is approximately 4 cm across. The blue box shows the approximate outline of the sample acquired for the present study. The yellow box shows the area shown in Fig. 1.



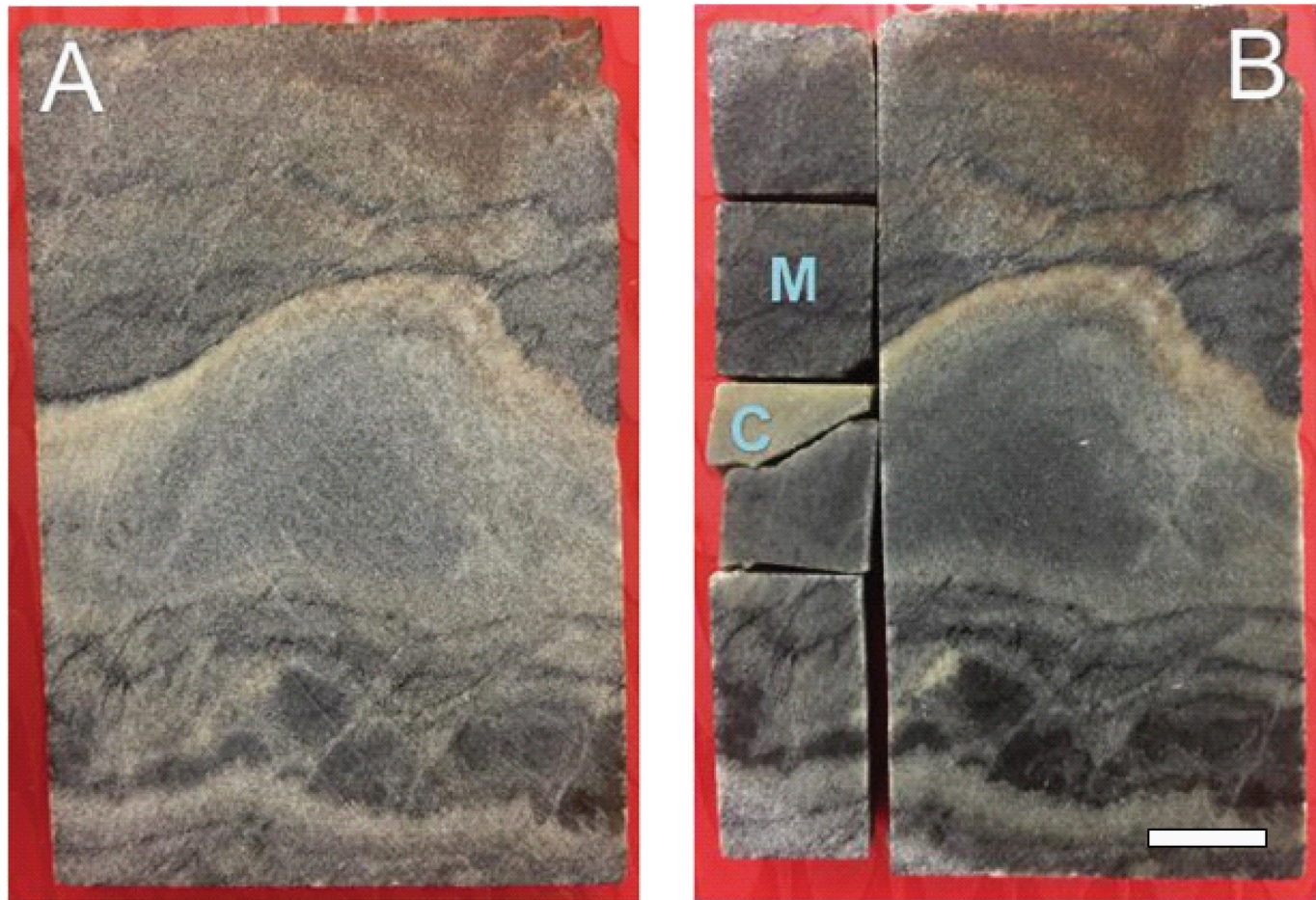
Extended Data Fig. 3 | Breccia at site C. **a**, Close-up view of breccia, from the previous study¹. Ch, chert; dol, dolomite. **b**, Larger field of view showing the same breccia block as in **a**, showing the location of the

elongated rod-like fabric (rodding) on the upper right side of the rock. **c**, Top view of the breccia-containing block from **a**—note the contrasting appearance of the rock fabric.



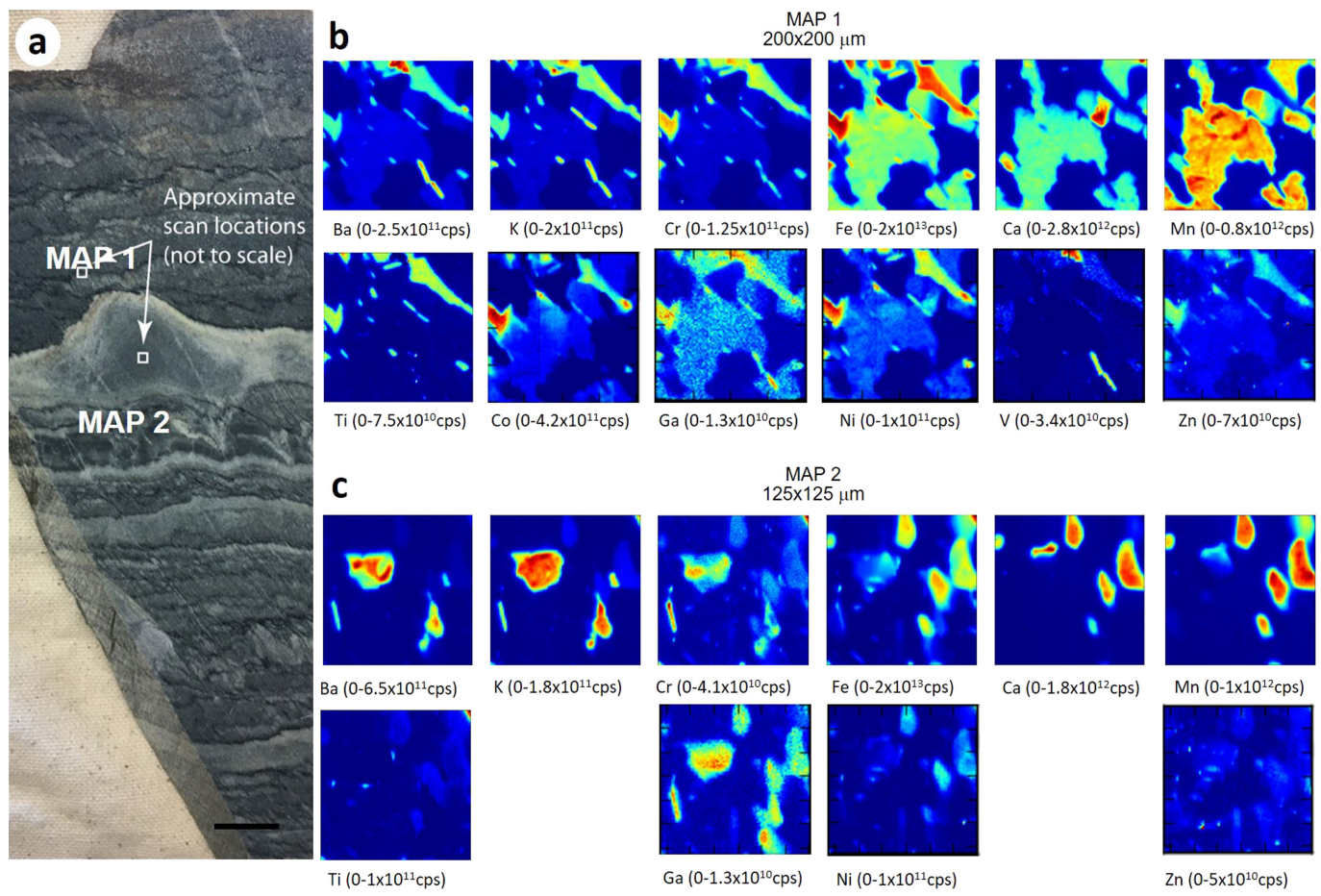
Extended Data Fig. 4 | Photographs of details from the deformation fabrics of site A. The photographs show details of the observed deformation fabrics on the cut and polished faces of all three pieces of the columnar sample that we collected from site A. Each piece was cut to show rock fabrics on orthogonal faces. **a**, Largest piece, which includes one of

the ‘stromatolites’ on the right face. Note contrasting fabrics on adjacent faces. **b–e**, Additional pieces of the rock sample, showing further examples of the contrasting rock fabrics. Green arrows on all images indicate the orientation of the spaced cleavage.



Extended Data Fig. 5 | Petrographic context of samples that were digested for REE + Y analyses. a, Slab sample before cutting. **b**, Slab sample after cutting. 'M' denotes the subsample from which analyses

'M3M' and 'M3C' were derived. 'C' denotes the subsample from which analyses 'C3M' and 'C3C' were derived. Scale bar, 10 mm.



Extended Data Fig. 6 | Synchrotron XRF element maps of the ISB sample. The distribution of trace elements relative to minerals is shown. **a**, Photograph of the sample. White squares show map locations. Scale bar, 10 mm. **b**, Distribution and X-ray intensity of detected elements for map 1. **c**, Distribution and X-ray intensity of detected elements for map 2.

b, c, X-ray intensity variations were used to colour the element maps. Blue, zero X-ray intensity; red, maximum X-ray intensity. X-ray intensity ranges (counts per second (cps)) are shown beneath each map. All maps are for K-shell X-rays except for Ba, which was detected using L-shell X-rays.

Extended Data Table 1 | REE + Y concentrations (p.p.m.) from acid digestion and ICP-MS analysis

I.D.	La	Ce	Pr	Nd	Sm	Eu	Gd	Tb	Dy	Y	Ho	Er		Tm	Yb	Lu
Carbonate fraction from “Stromatolite”																
C3C	0.414	0.530	0.070	0.332	0.082	0.040	0.113	0.017	0.113	1.335	0.025	0.072		0.010	0.100	0.011
Carbonate fraction from “Sediment”																
M3C	1.670	2.080	0.260	1.047	0.203	0.080	0.252	0.034	0.230	3.209	0.053	0.170		0.025	0.190	0.026
Silicate fraction from “Stromatolite”																
C3M	0.430	0.781	0.124	0.636	0.226	0.343	0.226	0.044	0.421	4.182	0.112	0.310		0.035	0.393	0.050
Silicate fraction from “Sediment”																
M3M	1.438	2.456	0.341	1.398	0.344	1.358	0.468	0.060	0.528	4.812	0.161	0.485		0.052	0.519	0.096

Reporting Summary

Nature Research wishes to improve the reproducibility of the work that we publish. This form provides structure for consistency and transparency in reporting. For further information on Nature Research policies, see [Authors & Referees](#) and the [Editorial Policy Checklist](#).

Statistical parameters

When statistical analyses are reported, confirm that the following items are present in the relevant location (e.g. figure legend, table legend, main text, or Methods section).

- | | |
|-------------------------------------|---|
| n/a | Confirmed |
| <input checked="" type="checkbox"/> | The <u>exact sample size</u> (<i>n</i>) for each experimental group/condition, given as a discrete number and unit of measurement |
| <input checked="" type="checkbox"/> | An indication of whether measurements were taken from distinct samples or whether the same sample was measured repeatedly |
| <input checked="" type="checkbox"/> | The statistical test(s) used AND whether they are one- or two-sided
<i>Only common tests should be described solely by name; describe more complex techniques in the Methods section.</i> |
| <input checked="" type="checkbox"/> | A description of all covariates tested |
| <input checked="" type="checkbox"/> | A description of any assumptions or corrections, such as tests of normality and adjustment for multiple comparisons |
| <input checked="" type="checkbox"/> | A full description of the statistics including <u>central tendency</u> (e.g. means) or other basic estimates (e.g. regression coefficient) AND <u>variation</u> (e.g. standard deviation) or associated <u>estimates of uncertainty</u> (e.g. confidence intervals) |
| <input checked="" type="checkbox"/> | For null hypothesis testing, the test statistic (e.g. <i>F</i> , <i>t</i> , <i>r</i>) with confidence intervals, effect sizes, degrees of freedom and <i>P</i> value noted
<i>Give P values as exact values whenever suitable.</i> |
| <input checked="" type="checkbox"/> | For Bayesian analysis, information on the choice of priors and Markov chain Monte Carlo settings |
| <input checked="" type="checkbox"/> | For hierarchical and complex designs, identification of the appropriate level for tests and full reporting of outcomes |
| <input checked="" type="checkbox"/> | Estimates of effect sizes (e.g. Cohen's <i>d</i> , Pearson's <i>r</i>), indicating how they were calculated |
| <input checked="" type="checkbox"/> | Clearly defined error bars
<i>State explicitly what error bars represent (e.g. SD, SE, CI)</i> |

Our web collection on [statistics for biologists](#) may be useful.

Software and code

Policy information about [availability of computer code](#)

Data collection

Provide a description of all commercial, open source and custom code used to collect the data in this study, specifying the version used OR state that no software was used.

n/a

Data analysis

Provide a description of all commercial, open source and custom code used to analyse the data in this study, specifying the version used OR state that no software was used.

n/a

For manuscripts utilizing custom algorithms or software that are central to the research but not yet described in published literature, software must be made available to editors/reviewers upon request. We strongly encourage code deposition in a community repository (e.g. GitHub). See the Nature Research [guidelines for submitting code & software](#) for further information.

Data

Policy information about [availability of data](#)

All manuscripts must include a [data availability statement](#). This statement should provide the following information, where applicable:

- Accession codes, unique identifiers, or web links for publicly available datasets
- A list of figures that have associated raw data
- A description of any restrictions on data availability

The datasets generated during and/or analysed during the current study are available from the corresponding author on reasonable request

Field-specific reporting

Please select the best fit for your research. If you are not sure, read the appropriate sections before making your selection.

- Life sciences Behavioural & social sciences Ecological, evolutionary & environmental sciences

For a reference copy of the document with all sections, see nature.com/authors/policies/ReportingSummary-flat.pdf

Ecological, evolutionary & environmental sciences study design

All studies must disclose on these points even when the disclosure is negative.

Study description	Geological and paleobiological field observations of putative Archean stromatolites, and analysis of returned samples
Research sample	Putative 3.7 billion year old stromatolites
Sampling strategy	observe in the field, collect sample from outcrop.
Data collection	Field note and photography, reflected and transmitted light microscopy/photography, geochemical analyses using micro-XRF, synchrotron XRF, mass spectroscopy
Timing and spatial scale	Sample was collected September 2016
Data exclusions	no exclusions
Reproducibility	The methods sections provide enough detail to allow anybody wishing to reproduce our analyses to do so.
Randomization	n/a
Blinding	n/a
Did the study involve field work?	<input checked="" type="checkbox"/> Yes <input type="checkbox"/> No

Field work, collection and transport

Field conditions	Clear, sunny, -8 Celsius
Location	Isua Structural Belt, Greenland (see location map in Extended Data Fig1)
Access and import/export	We were accompanied to the field site by Anette Juul-Nielsen Government of Greenland Ministry of Mineral Resources. They also issued a sampling permit
Disturbance	The sample was cut with a rock saw to minimize fracturing of the surrounding rock. The cuts were spaced to include only one of the structures, but large enough to get an adequate view of fabrics in the host rock. The sampling strategy was discussed with Anette prior to acquisition.

Reporting for specific materials, systems and methods

Materials & experimental systems

n/a	Involved in the study
<input type="checkbox"/>	Unique biological materials
<input type="checkbox"/>	Antibodies
<input type="checkbox"/>	Eukaryotic cell lines
<input checked="" type="checkbox"/>	Palaeontology
<input type="checkbox"/>	Animals and other organisms
<input type="checkbox"/>	Human research participants

Methods

n/a	Involved in the study
<input type="checkbox"/>	ChIP-seq
<input type="checkbox"/>	Flow cytometry
<input type="checkbox"/>	MRI-based neuroimaging

Unique biological materials

Policy information about [availability of materials](#)

Obtaining unique materials

n/a Describe any restrictions on the availability of unique materials OR confirm that all unique materials used are readily available from authors or from standard commercial sources (and specify these sources).

Antibodies

Antibodies used

n/a Describe all antibodies used in the study; as applicable, provide supplier name, catalog number, clone name, and lot number.

Validation

n/a Describe the validation of each primary antibody for the species and application, noting any validation statements on the manufacturer's website, relevant citations, antibody profiles in online databases, or data provided in the manuscript.

Eukaryotic cell lines

Policy information about [cell lines](#)

Cell line source(s)

n/a State the source of each cell line used.

Authentication

n/a Describe the authentication procedures for each cell line used OR declare that none of the cell lines used were authenticated.

Mycoplasma contamination

n/a Confirm that all cell lines tested negative for mycoplasma contamination OR describe the results of the testing for mycoplasma contamination OR declare that the cell lines were not tested for mycoplasma contamination.

Commonly misidentified lines (See [ICLAC register](#))

n/a Name any commonly misidentified cell lines used in the study and provide a rationale for their use.

Palaeontology

Specimen provenance

Isua Structural Belt, Greenland, at Nutman et al (2016) discovery locality, 65 deg 10'45"N, 49 deg 48'15"W

Specimen deposition

Jet Propulsion Laboratory, 4800 Oak Grove Dr, Pasadena, CA 91001 USA

Dating methods

n/a

Tick this box to confirm that the raw and calibrated dates are available in the paper or in Supplementary Information.

Animals and other organisms

Policy information about [studies involving animals; ARRIVE guidelines](#) recommended for reporting animal research

Laboratory animals

n/a For laboratory animals, report species, strain, sex and age OR state that the study did not involve laboratory animals.

Wild animals

n/a Provide details on animals observed in or captured in the field; report species, sex and age where possible. Describe how animals were caught and transported and what happened to captive animals after the study (if killed, explain why and describe method; if released, say where and when) OR state that the study did not involve wild animals.

Field-collected samples

n/a For laboratory work with field-collected samples, describe all relevant parameters such as housing, maintenance, temperature, photoperiod and end-of-experiment protocol OR state that the study did not involve samples collected from the field.

Human research participants

Policy information about [studies involving human research participants](#)

Population characteristics

n/a Describe the covariate-relevant population characteristics of the human research participants (e.g. age, gender, genotypic information, past and current diagnosis and treatment categories). If you filled out the behavioural & social sciences study design questionnaire and have nothing to add here, write "See above."

Recruitment

n/a Describe how participants were recruited. Outline any potential self-selection bias or other biases that may be present and how they likely to impact results.

ChIP-seq

Data deposition

- Confirm that both raw and final processed data have been deposited in a public database such as [GEO](#).
- Confirm that you have deposited or provided access to graph files (e.g. BED files) for the called peaks.

Data access links

May remain private before publication.

For "Initial submission" or "Revised version" documents, provide reviewer access links. For your "Final submission" document, provide **n/a** to the deposited data.

Files in database submission

Provide **n/a** of all files available in the database submission.

Genome browser session (e.g. [UCSC](#))

Provide a link to an anonymized genome browser session for "Initial submission" and "Revised version" documents only, to enable peer review. Write "no longer applicable" for "Final submission" documents.

Methodology

Replicates

Describe **n/a** experimental replicates, specifying number, type and replicate agreement.

Sequencing depth

Describe the sequencing depth for each experiment, providing the total number of reads, uniquely mapped reads, length of reads and whether they were paired- or single-end.

Antibodies

Describe the antibodies used for the ChIP-seq experiments; as applicable, provide supplier name, catalog number, clone name, and lot number.

Peak calling parameters

Specify the command line program and parameters used for read mapping and peak calling, including the ChIP, control and index files used.

Data quality

Describe the methods used to ensure data quality in full detail, including how many peaks are at FDR 5% and above 5-fold enrichment.

Software

Describe the software used to collect and analyze the ChIP-seq data. For custom code that has been deposited into a community repository, provide accession details.

Flow Cytometry

Plots

Confirm that:

- The axis labels state the marker and fluorochrome used (e.g. CD4-FITC).
- The axis scales are clearly visible. Include numbers along axes only for bottom left plot of group (a 'group' is an analysis of identical markers).
- All plots are contour plots with outliers or pseudocolor plots.
- A numerical value for number of cells or percentage (with statistics) is provided.

Methodology

Sample preparation

Describe the sample preparation, detailing the biological source of the cells and any tissue processing steps used.

Instrument

Identify the instrument used for data collection, specifying make and model number.

Software

Describe the software used to collect and analyze the flow cytometry data. For custom code that has been deposited into a community repository, provide accession details.

Cell population abundance

Describe the abundance of the relevant cell populations within post-sort fractions, providing details on the purity of the samples and how it was determined.

Gating strategy

Describe the gating strategy used for all relevant experiments, specifying the preliminary FSC/SSC gates of the starting cell population, indicating where boundaries between "positive" and "negative" staining cell populations are defined.

- Tick this box to confirm that a figure exemplifying the gating strategy is provided in the Supplementary Information.

Magnetic resonance imaging

Experimental design

Design type

Indicate task or resting state, event-related or block design.

Design specifications	<i>Specify the number of blocks, trials or experimental units per session and/or subject, and specify the length of each trial or block (e.g. trials are blocked) and interval between trials.</i> n/a
Behavioral performance measures	<i>State number and/or type of variables recorded (e.g. correct button press, response time) and what statistics were used to estimate that the subjects were performing the task as expected (e.g. mean, range, and/or standard deviation across subjects).</i> n/a
Acquisition	
Imaging type(s)	<i>Specify functional, structural, diffusion, perfusion.</i> n/a
Field strength	<i>Specify Tesla.</i> n/a
Sequence & imaging parameters	<i>Specify the pulse sequence type (gradient echo, spin echo, etc.), imaging type (EPI, spiral, etc.), field of view, matrix size, slice thickness, orientation and TE/TR/flip angle.</i> n/a
Area of acquisition	<i>State whether a whole brain scan was used OR define the area of acquisition, describing how the region was determined.</i> n/a
Diffusion MRI	<input checked="" type="checkbox"/> Used <input type="checkbox"/> Not used
Preprocessing	
Preprocessing software	<i>Provide detail on software version and revision number and on specific parameters (model/functions, brain extraction, segmentation, smoothing kernel size, etc.).</i> n/a
Normalization	<i>If data were normalized/standardized, describe the approach(es); specify linear or non-linear and define image types used for transformation OR indicate that data were not normalized and explain rationale for lack of normalization.</i> n/a
Normalization template	<i>Describe the template used for normalization/transformation, specifying subject space or group standardized space (e.g. original MNI, MNI152, MNI1305, ICBM152) OR indicate that the data were not normalized.</i> n/a
Noise and artifact removal	<i>Describe your procedure(s) for artifact and structured noise removal, specifying motion parameters, tissue signals and physiological signals (heart rate, respiration).</i> n/a
Volume censoring	<i>Define your software and/or method and criteria for volume censoring, and state the extent of such censoring.</i> n/a
Statistical modeling & inference	
Model type and settings	<i>Specify type (e.g. univariate, multivariate, RSA, predictive, etc.) and describe essential details of the model at the first and second levels (e.g. fixed, random or mixed effects; drift or auto-correlation).</i> n/a
Effect(s) tested	<i>Define precise effect in terms of the task or stimulus conditions instead of psychological concepts and indicate whether ANOVA or factorial designs were used.</i> n/a
Specify type of analysis:	<input type="checkbox"/> Whole brain <input type="checkbox"/> ROI-based <input type="checkbox"/> Both
Statistic type for inference (See Eklund et al. 2016)	<i>Specify voxel-wise or cluster-wise and report all relevant parameters for cluster-wise methods.</i> n/a
Correction	<i>Describe the type of correction and how it is obtained for multiple comparisons (e.g. FWE, FDR, permutation or Monte Carlo). n/a</i>
Models & analysis	
n/a	Involved in the study
<input checked="" type="checkbox"/>	Functional and/or effective connectivity
<input checked="" type="checkbox"/>	Graph analysis
<input checked="" type="checkbox"/>	Multivariate modeling or predictive analysis
Functional and/or effective connectivity	<i>Report the measures of dependence used and the model details (e.g. Pearson correlation, partial correlation, mutual information).</i> n/a
Graph analysis	<i>Report the dependent variable and connectivity measure, specifying weighted graph or binarized graph, subject-level or node-level, and the global and/or node summaries used (e.g. clustering coefficient, efficiency, etc.). n/a</i>
Multivariate modeling and predictive analysis	<i>Specify independent variables, features extraction and dimension reduction, model, training and evaluation metrics. n/a</i>